Intermetal bonding network in two-dimensional tetranuclear clusters

ARTICLE *in* JOURNAL OF THE AMERICAN CHEMICAL SOCIETY · JULY 1990

Impact Factor: 12.11 · DOI: 10.1021/ja00170a012

2 AUTHORS:

Carlo Mealli
Italian National Research Council
245 PUBLICATIONS **5,012** CITATIONS
SEE PROFILE

Davide M Proserpio
University of Milan
216 PUBLICATIONS **11,645** CITATIONS
SEE PROFILE

Reprinted from the Journal of the American Chemical Society, 1990, 112.

Intermetal Bonding Network in Two-Dimensional Tetranuclear Clusters

Carlo Mealli* and Davide M. Proserpio

Contribution from the Istituto per lo Studio della Stereochimica ed Energetica dei Composti di Coordinazione, C.N.R., Via J. Nardi 39, I-50132 Firenze, Italy. *Received October 9, 1989*

Abstract: The present study deals with the small number of structurally characterized 64 → 60e⁻ tetranuclear clusters containing metals of the groups 7 → 10 and having in common the primary feature of planarity. The M_4 skeleton has a variety of shapes: square, rhombus, or more generally quadrilateral. Empirical electron counting rules do not always provide a sufficient description of the bonding in these two-dimensional compounds nor is the viewpoint unique for different cases. In order to determine the electronic distribution, hence the trends of the M_4 skeleton to deform, extended Hückel calculations have been carried out for a number of models. The nature of the outer M–M σ interactions and the distribution of the metal lone pairs are illustrated for 64e⁻ square clusters. Then, it is shown that 62e⁻ $M_4(CO)_{16}$ rhombuses correlate ideally with 64e⁻ squares through the formation of one diagonal bond. Five M–M bonds are also ascertained in the 62e⁻ quadrilateral $Os_4(CO)_{15}$ that is short one ligand. In any case, the fifth bond is shown to involve "t_{2g}" orbitals in an unforeseen way. The distribution of the M–M bonds in 64e⁻ clusters, containing π-donor coplanar phosphido bridges, is irregular. In $Ru_4(CO)_{13}(\mu\text{-}PPh_2)_2$, formed by two condensed triangles sharing one side, only two outer consecutive Ru–Ru linkages have bond order 1, whereas the other three (including the quadrilateral's diagonal) are assigned bond order 2/3. In $Ru_4(CO)_{10}(\mu\text{-}PPh_2)_4$ the M_4 bonding network is something intermediate between two limiting viewpoints. The first one assigns a total of three bonds to the four sides of the Ru_4 rhombus. The fourth linkage, coinciding with one diagonal, is best described as an uncommon *four electron/three orbitals* bond. The other description indicates that a fourth cyclic M–M bond is formed at expenses of part of the M–P bridge-bonding network. The theoretical result has also an experimental confirmation. Finally, there are planar tetranuclear clusters having all of the metal atoms square planarly coordinated by ligands and a reduced number of M–M connectivities. Among the latter, $Ni_4(\mu\text{-}SR)_8$ (64 electrons) has a square Ni_4 skeleton but no M–M bond, whereas $Pd_4(\mu\text{-}CO)_4(\mu\text{-}CH_3CO_2)_4$, with 60 electrons, is a parallelogram with two M–M bonds at those sides doubly bridged by the carbonyl ligands.

Introduction

The use of the *isolobal analogy* concept[1] simplifies the understanding of complex molecules. In the realm of organometallics one or more metal fragments with the proper electron count are considered to be the inorganic substituents of organic precursors. If all of the organic fragments are substituted for, then the realm of clusters is accessed. Most clusters can be recognized as being built up of catalogued metal fragments for which there exist isolobal analogues.[2]

A possible shortcoming of the analogy depends on the fact that metal atoms have nine rather than four atomic orbitals at disposal. Such a richness not only offers a large flexibility to the hybridization of the frontier orbitals but also, under certain circumstances, allows additional bonding capabilities to the metals. The latter can be specifically exerted in the construction of intermetal bonding networks, i.e., clusters.

To substantiate the previous idea, we mention the findings of a recent MO analysis performed by us on the dimer $(CO)_3Fe(\mu\text{-}CO)_3Fe(CO)_3$.[3] In this bioctahedron with one shared face, each metal uses six atomic orbitals to achieve the hexacoordination with terminal and bridging ligands. The direct Fe–Fe bond is formed through the use of one of the "t_{2g}" nonbonding orbitals from each metal, a possibility not available to nontransition fragments. The point is not a restatement of the Hoffmann idea[1] that "t_{2g}" orbitals do occasionally concur to the formation of isolobal hybrids, rather a "t_{2g}" orbital is seen to form a bond in a new, unforeseen way. Additional examples will be provided throughout this paper.

Precious information about the bonding and stability of metal clusters is obtainable from empirical rules based on the count of the electrons.[4] Thus, the effective atomic number (EAN) rule [$m = (18n - k)/2$] predicts the number (m) of M–M bonds as a function of the total electron count (k) and of the number of metals (n). The polyhedral skeleton electron pair theory of Wade and Mingos (PSEPT)[5] combines the power of the electron counting with that stemming from the isolobal analogy. Teo[6] has introduced the topological electron counting scheme (TEC) that uses an adjusting parameter to be defined case by case. Lahuer,[7] on the basis of MO calculations, provides general guidelines to derive the various electron counts for different polyhedra. In principle, it is possible to distinguish two main groups of MOs (cluster valence molecular orbitals [CVMOs] and high lying antibonding orbitals [HLAOs]). The number of electrons needed to populate in full the lower CVMOs corresponds also to the most stable electron configuration of the cluster.

In spite of their utility, not all of the previous approaches are successful all of the time. When the *magic numbers* predicted by the rules do not fit, ad hoc considerations are introduced to override the problem, but the loss of generality is evident.

A possible problem with the Lahuer's approach is that in some cases the HOMO–LUMO gap can be small. The assignment of a specific frontier level either to CVMOs or HLAOs becomes uncertain. Consequently, it is also difficult to assess whether a typified cluster is more stable with n or with $n + 2$ electrons. As an example, in carbonyl octahedral clusters an a_{2g} multinoded antibonding combination of metal δ orbitals is not sufficiently destabilized.[8] Thus the level is assigned to the group of CVMOs that, consequently, sum up to 43 (=86 electrons). By contrast octahedral clusters having π-donor μ_3-capping ligands {e.g., $[Mo_6(\mu_3\text{-}L_8)L_2]^{2-}$, L = Cl, OR} are stable with 84 electrons because the antibonding character of a_{2g} is now sufficiently enhanced for it to enter the group of HLAOs.[9]

A similar dichotomy occurs for two-dimensional tetranuclear clusters with formula M_4L_{16}, e.g., $Os_4(CO)_{16}$,[10] **2**, and $[Re_4(CO)_{16}]^{2-}$,[11] **10**, shown as I and II, respectively. In these, the 32nd highest MO is not greatly separated from the lower 31 MOs. The

(1) Hoffmann, R. *Angew. Chem., Int. Ed. Engl.* **1982**, *21*, 711.
(2) Evans, D. G. *J. Chem. Soc., Chem. Commun.* **1983**, 675.
(3) Mealli, C.; Proserpio, D. M. *J. Organomet. Chem.* **1990**, 386, 203.
(4) For recent reviews, see: Kharas, K. C. C.; Dahl, L. F. *Adv. Chem. Phys.* **1988**, *70*, 1. Owen, S. M. *Polyhedron* **1988**, *7*, 253. Mingos, D. M. P.; Johnson, R. L. *Struct. Bonding* **1987**, *68*, 29.
(5) Mingos, D. M. P. *Nature Phys. Sci. (London)* **1972**, *236*, 99. Wade, K. *Adv. Inorg. Chem. Radiochem.* **1976**, *18*, 1.
(6) Teo, B. K. *Inorg. Chem.* **1984**, *23*, 1251; **1985**, *24*, 1627, 4209.
(7) Lauher, J. W. *J. Am. Chem. Soc.* **1978**, *100*, 5305.
(8) Mingos, D. M. P.; Johnson, R. L. *Inorg. Chem.* **1986**, *25*, 1661.
(9) Chisholm, M. H.; Clark, D. L.; Hampden-Smith, M. J.; Hoffman, D. H. *Angew. Chem., Int. Ed. Engl.* **1989**, *28*, 432.
(10) Johnston, V. J.; Einstein, F. W. B.; Pomeroy, R. K. *J. Am. Chem. Soc.* **1987**, *109*, 8111.
(11) Churchill, M. R.; Bau, R. *Inorg. Chem.* **1968**, *7*, 2606. Ciani, G.; D'Alfonso, G.; Freni, M.; Romiti, P.; Sironi, A. *J. Organomet. Chem.* **1978**, *157*, 199.

0002-7863/90/1512-5484$02.50/0

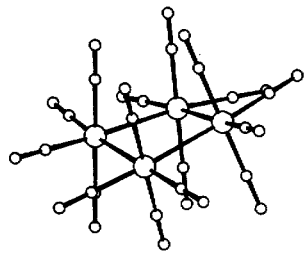

$Os_4(CO)_{16}$, **2**

I

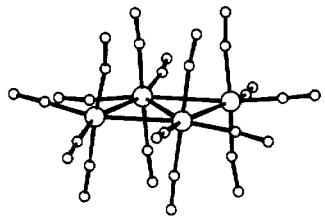

$[Re_4(CO)_{16}]^{2-}$, **10**

II

ΔE, at the level of semiempirical MO methods, is sensitive to the choice of the parameters as well as to the geometry of the quadrilateral. Regardless of the difficult assignment of the 32nd level either to CVMOs or HLAOs, Lahuer defines two main geometric categories, namely D_{4h} (square) and D_{2h} (rhombus), that should be stable with 64 and 62 electrons, respectively.[7]

The lack of a conceptual continuity between D_{4h} and D_{2h} categories is also transparent in other approaches, for example, the PSEP theory.[5] Arachno compounds should in principle obey the $7n + 3$ rule that provides the total number of electron pairs. This seems to work for $48e^-$ triangular species such as $Os_3(CO)_{12}$, but it predicts 62 electrons for four-membered rings, such as $Os_4(CO)_{16}$. Moreover, the rule's applicability is questionable since the single fragments are not conical (ML_4 with C_{2v} symmetry) nor does the cluster have triangular faces (deltahedral). In the attempt to extend the theory to nonconical fragments, Mingos and Evans[12] subdivide 64 and $62e^-$ clusters in two different classes. While the former class includes rings for which a 16×4 electron count is predictable (the $16n$ rule for the total electron count applies for triangules, squares, etc.), $62e^-$ species, such as $[Re_4(CO)_{16}]^{2-}$ (a rhombus seen as a triangle bridged at one side), require the extension of the capping principle from three-dimensional to two-dimensional clusters. Finally, the application of the TEC schemes[6] to two-dimensional clusters, although potentially successful, is somewhat hard to handle since as many as four different variables need to be defined.

Tetranuclear planar clusters are not limited to the square/rhombus dichotomy. A couple of compounds, recently reported by Carty et al.[13] (one of them has related analogues in the literature[14,15]), have a puzzling M–M bonding distribution. In the $64e^-$ species $Ru_4(CO)_{13}(\mu\text{-}PPh_2)_2$,[13] **7** (see III), with two bridging phosphido groups, the Ru_4 skeleton has a quadrilateral shape with two different types of Ru–Ru cyclic bonds.

In the other $64e^-$ species, $Ru_4(CO)_{10}(\mu\text{-}PPh_2)_4$,[13] **6** (see IV), with four phosphide bridges, the M_4 shape is a rhombus, but at variance with the classic D_{2h} $62e^-$ rhombus, $[Re_4(CO)_{16}]^{2-}$, **10**, one diagonal is shorter than the four sides. In turn, the latter are all too long to be Ru–Ru single bonds. It is likely that the bond order is fractional for some of the Ru–Ru linkages in **6** and **7**.

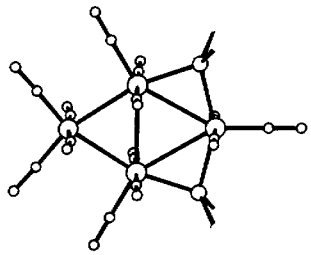

$Ru_4(CO)_{13}(\mu\text{-}PPh_2)_2$, **7**

III

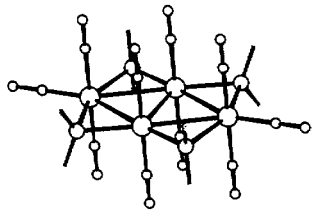

$Ru_4(CO)_{10}(\mu\text{-}PPh_2)_4$, **6**

IV

Moreover in these as well as in **10** the in-plane M_4 bonds have both perimetric and transannular distribution, different from square $64e^-$ clusters and from the simplest four-membered ring such as cyclobutane. This point is noteworthy as the M_4 assembly in **7** and **6** seems to embody already some features typical of the bulk metals.

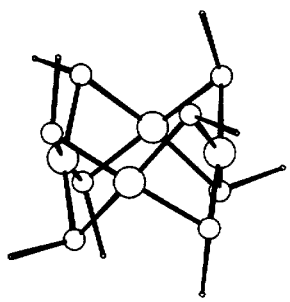

$Ni_4(\mu\text{-}SC_6H_{11})_8$, **4**

V

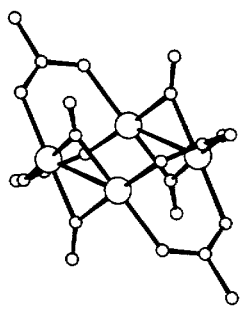

$Pd_4(\mu\text{-}CH_3CO_2)_4(\mu\text{-}CO)_4$, **16**

VI

Finally, there are examples of planar clusters that contain either none or only two M–M bonds. In these compounds, that have formulas $Ni_4(\mu\text{-}SR)_8$,[16] **4**, and $Pd_4(\mu\text{-}CO)_4(\mu\text{-}CH_3CO_2)_4$,[17] **16** (see V and VI, respectively), the metal atoms are all square-planar coordinated by ligands. Are there some residual interactions that

(12) Evans, D. G.; Mingos, D. M. P. *J. Organomet. Chem.* **1982**, *240*, 321; *Organometallics* **1983**, *2*, 435.
(13) Hogart, G.; Phillips, J. A.; Van Gastel, F.; Taylor, N. J.; Marder, T. B.; Carty, A. J. *J. Chem. Soc., Chem. Commun.* **1988**, 1570.
(14) Carty, A. J.; MacLaughlin, S. A.; Van Wagner, J.; Taylor, N. J. *Organometallics* **1982**, *1*, 1013. Carty, A. J. *Pure Appl. Chem.* **1982**, *54*, 113.
(15) Churchill, M. R.; Bueno, C.; Young, D. A. *J. Organomet. Chem.* **1981**, *213*, 139.
(16) Kriege, M.; Henkel, G. *Z. Naturforsch.* **1987**, *42B*, 1121.
(17) Moiseev, I. I.; Stromnova, T. A.; Vargaftig, M. N.; Mazo, G. Ja.; Kuz'mina, L. G.; Struchkov, Yu. T. *J. Chem. Soc., Chem. Commun.* **1978**, 27.

Table I. Features of Uncapped Tetranuclear Planar Clusters[a]

				M–M, Å (av)			ref
64 Electrons							
M_4L_{16}	1	$Pt_4(\mu\text{-}CH_3CO_2)_8$	sq	s = 2.494 (4)			19
	2	$Os_4(CO)_{16}$	sq	s = 2.99 (1)			10
	3	$[Re_4(\mu_4\text{-}C)(CO)_{15}I]^-$	sq	s = 3.00 (1)			20
	4	$Ni_4(\mu\text{-}SC_6H_{11})_8$	sq	s = 2.685 (6)			16
	5	$Pd_4(\mu\text{-}CCl_3CO_2)_4(\mu\text{-}t\text{-}BuOO)_4$	sq	s = 2.917 (7)			21
$M_4L_m(\mu\text{-}E)_n$	6	$Ru_4(CO)_{10}(\mu\text{-}PPh_2)_4$	rh	s = 3.05 (1)	d = 2.8355 (7)		13
	7	$Ru_4(CO)_{13}(\mu\text{-}PPh_2)_2$	qu	s = 2.91 (1)	b = 3.17 (2)	d = 3.1335 (4)	13
	8	$Ru_4(CO)_{13}(\mu\text{-}PPh_2)(\mu\text{-}\eta^2\text{-}C{\equiv}C\text{-}t\text{-}Bu)$	qu	s = 2.89 (2)	b = 3.18 (3)	d = 3.024 (1)	14
	9	$Ru_3Fe(CO)_{13}(\mu\text{-}PPh_2)_2$	qu	s_{Ru-Fe} = 2.864 (5)	b_{Ru-Ru} = 3.16 (2)	d_{Ru-Ru} = 3.098 (1)	15
62 Electrons							
M_4L_{16}	10	$[Re_4(CO)_{16}]^{2-}$	rh	$s = d$ = 2.99 (3)			11
	11	$Os_4(CO)_{12}(\mu\text{-}CF_3CO_2)_2$	pa	s = 2.779 (2)	s = 2.894 (2)	d = 2.861 (2)	22
	12	$Os_3ReH(CO)_{15}$	rh	s = 2.957 (1)	d_{Os-Re} = 2.944 (1)		23
M_4L_{15}	13	$Os_4(CO)_{15}$	qu	$s_{ML_3-ML_4}$ = 2.772 (1)	$s_{ML_4-ML_4}$ = 2.997 (1)	$d_{ML_3-ML_4}$ = 2.948 (1)	24
	14	$Os_4(CO)_{14}(PMe_3)$	qu	$s_{ML_3-ML_4}$ = 2.781 (4)	$s_{ML_4-ML_4}$ = 3.00 (2)	$d_{ML_3-ML_4}$ = 2.935 (2)	25[a,b]
	15	$Os_3Ir(CO)_{12}(\eta^5\text{-}C_5Me_5)$	qu	s_{ML_3-Ir} = 2.703 (2)	$s_{ML_3-ML_4}$ = 2.796 (2)		
				s_{ML_4-Ir} = 2.939 (2)	$s_{ML_4-ML_4}$ = 2.994 (2)	$d_{ML_3-ML_4}$ = 2.909 (2)	24
60 Electrons							
	16	$Pd_4(\mu\text{-}CH_3CO_2)_4(\mu\text{-}CO)_4$	pa	s = 2.909 (1)	b = 2.663 (1)		17

[a] Legend: sq = square, rh = rhombus, qu = quadrilateral, pa = parallelogram, d = diagonal, s = side, b = bridged side, ML_3 = planar T-shaped metal fragment, ML_4 = butterfly metal fragment with C_{2v} local symmetry.

force the coplanarity of the M_4 skeleton?

Table I summarizes the structural features of the M_4 skeletons in all of the hit entries of the Cambridge Structural Database.[18] For a quick identification of the compounds under consideration, the reader should always refer to the numbering scheme in Table I.

On the basis of the experimental data and by carrying out EHMO calculations[26] with FMO analysis,[27] we have tackled a systematic analysis of the chemical bonding. As a criterion, a larger importance is attributed to the symmetry of the MOs rather than to the numerical quantities associated with them. Also, an effort has been done to determine the role of each MO relative to the other MOs in the overall picture. The purpose is that of singling out the metal–metal bonds in the different cases by extracting from the MO scheme all the M–M bonding and antibonding levels as well as the distribution of metal lone pairs. Already, we have applied these guidelines to study the unique paramagnetic 56e⁻ planar tetranuclear cluster $Fe_4(CO)_8(pyridine)_4$.[28]

Results

Outer σ-Bonding Network in Four-Membered Rings. Let us think of square-planar transition-metal clusters as the inorganic rings equivalent to cyclobutane.[29] The simplification holds as far as four L_nM fragments, similarly to four CH_2 groups, are able to provide two singly occupied orbitals (one radial σ and one tangential π) and to give rise to a pattern of four filled (bonding) below four empty (antibonding) MOs, see VII.

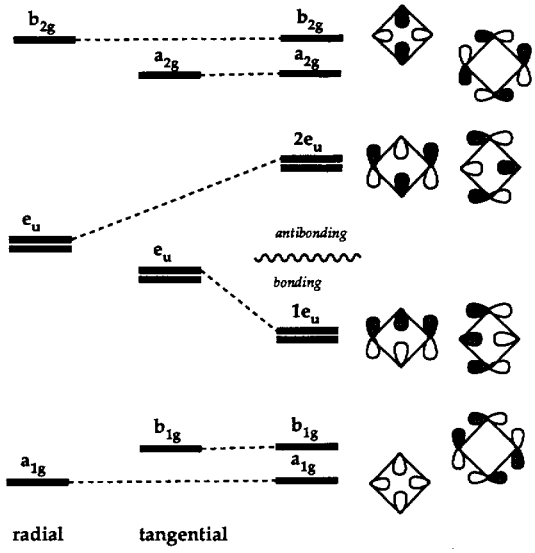

VII

Importantly, the formation of the four cyclic M–M bonds is afforded by the mixing of the two e_u symmetry combinations originally carrying separated σ and π characters, respectively.[29] The rules that govern the mixing between orbitals of equal symmetry descend from the second-order perturbation theory:[30] the larger the mixing, the larger the gap between bonding and antibonding combinations. Through the radial–tangential mixing, the initially nonbonding e_u levels (centered on pairs of trans diagonal atoms) acquire bonding/antibonding character with increased energy gap.

In the above context, Lauher[31] has recently pointed out that for the square cluster **2** (see I) the mixing of the different e_u levels is null and does not allow the formation of four Os–Os single bonds (vide infra). Experimental support to such a viewpoint would be provided not only by the scarce stability of **2** but also by the long intermetal separations of 2.99 (1) Å. As a comparison, the Os–Os bonds are at least 0.1 Å shorter in the triangular Os_3L_{12} species.[32,25b] By contrast, the closely relatable cluster $Pt_4(\mu$-

(18) Cambridge Crystallographic Data Centre, University Chemical Laboratory, Lensfield Road, Cambridge CB2 1EW, U.K., copyright 1988.
(19) Carrondo, M. A. A. F. de C. T.; Skapski, A. C. *Acta Crystallogr., Sect. B* **1978**, *B34*, 1857, 3576.
(20) Berringhelli, T.; Ciani, G.; D'Alfonso, G.; Sironi, A.; Freni, M. *J. Chem. Soc., Chem. Commun.* **1985**, 978.
(21) Mimoun, H.; Charpentier, R.; Mitschler, A.; Fischer, J.; Weiss, R. *J. Am. Chem. Soc.* **1980**, *102*, 1047.
(22) Diebold, M. P.; Drake, S. R.; Johnson, B. F. G.; Lewis, J.; McPartlin, M.; Powell, H. *J. Chem. Soc., Chem. Commun.* **1988**, 1358.
(23) Churchill, M. R.; Hollander, F. J. *Inorg. Chem.* **1977**, *16*, 2493.
(24) Johnston, V. J.; Einstein, F. W. B.; Pomeroy, R. K. *J. Am. Chem. Soc.* **1987**, *109*, 7220.
(25) (a) Martin, R. L.; Einstein, F. W. B.; Pomeroy, R. K. *J. Am. Chem. Soc.* **1986**, *108*, 338. (b) Martin et al. *Organometallics* **1988**, *7*, 294.
(26) Hoffmann, R.; Lipscomb, W. N. *J. Chem. Phys.* **1962**, *36*, 2179, 3489. Hoffmann, R. *J. Chem. Phys.* **1963**, *39*, 1397.
(27) Hoffmann, R.; Fujimoto, H.; Swenson, J. R.; Wan, C.-C. *J. Am. Chem. Soc.* **1973**, *95*, 7644. Hoffmann, R.; Fujimoto, H. *J. Phys. Chem.* **1974**, *78*, 1167.
(28) Mealli, C.; Proserpio, D. M.; Fachinetti, G.; Funaioli, T.; Fochi, G.; Zanazzi, P. F. *Inorg. Chem.* **1989**, *28*, 1122.
(29) Albright, T. A.; Burdett, J. K.; Whangbo, M. H. *Orbital Interactions in Chemistry*; Wiley: New York, 1985.
(30) Hoffmann, R. *Acc. Chem. Res.* **1971**, *4*, 1.
(31) Lauher, J. W. *Int. J. Quant. Chem., Quant. Chem. Sym.* **1988**, *22*, 309.
(32) Churchill, M. R.; DeBoer, B. G. *Inorg. Chem.* **1977**, *16*, 878.

Chart I

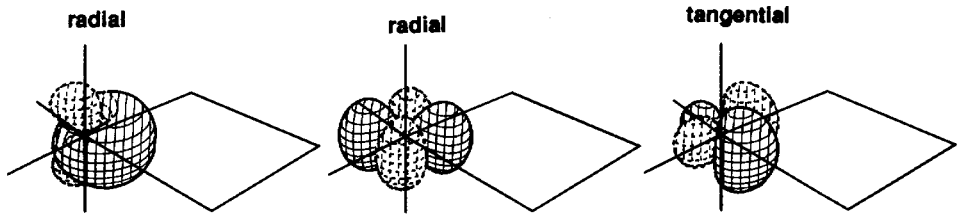

IX X XI

$CH_3CO_2)_8$,[19] **1** (see VIII), in which the Pt–Pt separation is as short as 2.494 (4) Å, would be largely stabilized by the acetato bridges. Independently from this latter argument, the MO analysis, presented in this paper, indicates the presence of four well-defined M–M single bonds for the general class of 64e⁻ square clusters.

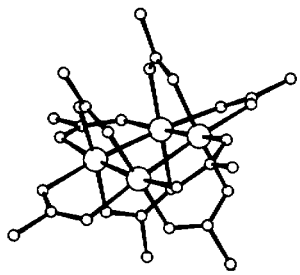

$Pt_4(\mu\text{-}CH_3CO_2)_8$, **1**

VIII

The model $Os_4H_{16}^{16-}$ allows a correct analysis of the symmetry properties from calculations. More realistic models with CO ligands provide in some cases numerical results more consistent with the experimental data, and their use will be mentioned.

As a general statement for cluster compounds, the MOs near the Fermi level have metal (d) character, largely based on the fact that the metal–ligand interactions are stronger than any metal (d)–metal (d) interaction. A possible question is whether the orbitals of the d band can carry any M–M bonding character and how one can distinguish the latter from the metal lone pairs. The diagram (Figure 1) for the interaction between pairs of nonadjacent ML_4 fragments[29] (with local C_{2v} symmetry and isolobal with CH_2) is most informative in this respect.

Consider that each metal atom uses four of its nine orbitals to make four M–L bonds. Thus each ML_4 fragment is left with five MOs, two of which (the "t_{2g}" lone pairs xz and yz with $d\pi_\perp$ and $d\delta$ characters) are extraneous to the in-plane M_4 σ bonding pattern. Ultimately, each fragment has three FMOs in the M_4 equatorial plane, two of which are σ-radial (the high-lying sp hybrid, IX, and the "t_{2g}" x^2–y^2-orbital, X) and one is π-tangential (the hybridized xy-type orbital, XI).

By combining together two trans diagonal ML_4 fragments, the orbitals IX–XI form in-phase and out-of-phase combinations. The latter FMOs correspond to the 1σ, $1\sigma^*$, π, π^* and 2σ, $2\sigma^*$ on both sides of Figure 1. At the center of the Figure 1, notice a double set of radial MOs (a_{1g}, e_u, b_{2g}) with respect to the single set in pattern VII. Thus a total of three e_u levels do exist, all mixed with each other.

Lauher forwards the argument[31] that the relative nodal properties of the σ and π levels (pure x^2-y^2 and xy, respectively) make null their crosssed overlap. This is schematized in XII relative to one of the many possible linear combinations having e_u symmetry.

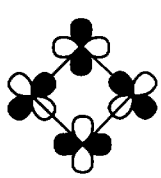

XII

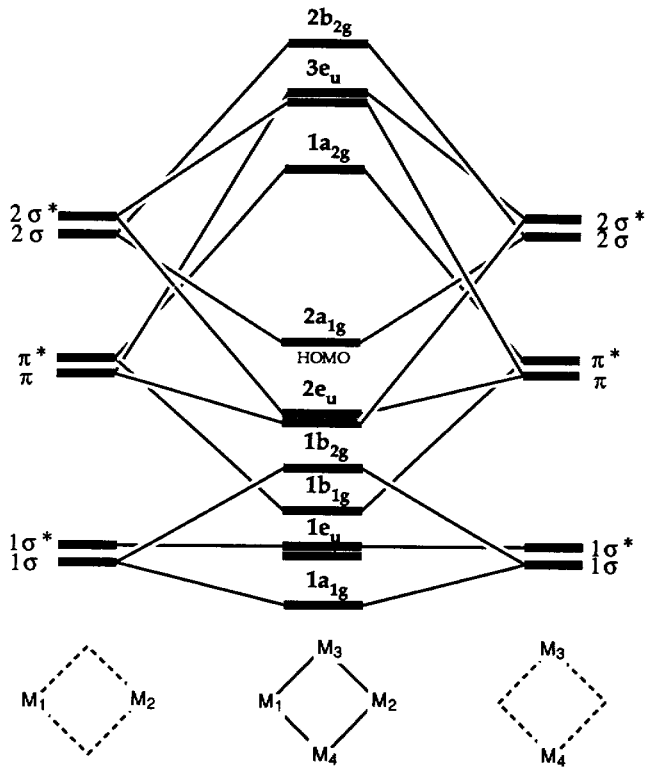

Figure 1. General diagram for the construction of the MOs of square clusters of the type M_4L_{16} from pairs of orthogonally oriented $L_4M\cdots ML_4$ fragments.

It is clear from Figure 1 that all of the symmetry combinations of x^2-y^2 ($1a_{1g}$, $1e_u$, $1b_{2g}$) stay almost unaffected at low energy. By contrast, the calculations indicate significantly positive overlap populations (OP = 0.31) for any of the two interactions of e_u type between $2\sigma^*$ and π FMOs. Filled bonding and empty antibonding levels ($2e_u$ and $3e_u$, respectively) are hence originated and account for two of the four cyclic M–M bonds. A representation of one $2e_u$ member is reported in XIII. In contrast with the hypothesized situation XII, the positive ovrlap stems from the hybridization of both the radial (IX) and tangential (XI) FMOs at each ML_4 fragment.

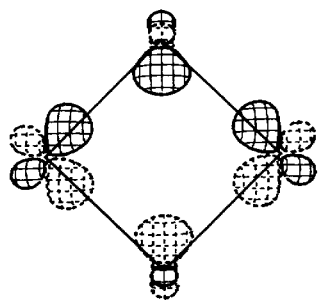

XIII

The remaining two cyclic M–M bonds are due to $\langle 2\sigma/2\sigma\rangle$ and $\langle \pi^*/\pi^*\rangle$ bonding interactions that have OP values of 0.48 and 0.39, respectively. The former interaction ($2a_{1g}$) involves all

in-pointing lobes (XIV) and the latter one ($1b_{1g}$) all out-pointing lobes (XV).

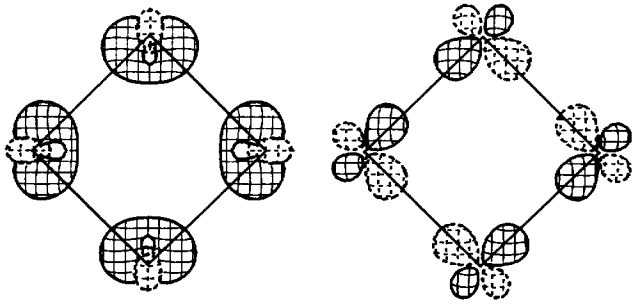

XIV XV

In summary, the filled levels $1b_{1g}$, $2e_u$, and $2a_{1g}$ are the four M_4 bonding MOs that, with their antibonding counterparts, ensure the existence of four single M–M bond in $64e^-$ square rings. The levels $1a_{1g}$, $1e_u$, and $1b_{2g}$ are the four metal σ-lone pairs that add to the eight lone pairs having $d\pi_\perp$ and $d\delta$ characters (not reported). These 12 lone pairs correspond to the four "t_{2g}" sets associated with all of the ML_4 fragments. The in-plane electron distribution of the twelve MOs of Figure 1 can be schematized as in XVI, with four lone pairs and eight cyclic orbitals.

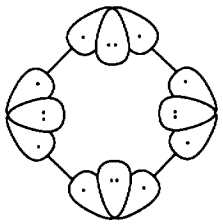

XVI

It has been pointed out[10] that $Os_4(CO)_{16}$ is more unstable than $Os_3(CO)_{12}$ where the Os–Os bonds are shorter. The point is confirmed by a specific MO calculation for a model of $Os_3(CO)_{12}$ in which the same intermetal separations as in $Os_4(CO)_{16}$ (=2.9 Å) were used. In agreement with the experimental data, the Os–Os overlap population is significantly greater in the trinuclear species (0.210 vs 0.190). The difference is attributable to a better overlap between the radial lobes (IX) of the ML_4 fragments in $Os_3(CO)_{12}$. In fact the distance of each metal from the center of the ring is only 1.67 Å, whereas it is 2.05 Å in the square compound. By contrast, the σ-radial lone pairs of the ML_4 fragments (those appearing in XVI) become a source of instability in the triangle as they are forced to stay in close proximity. As previously pointed out,[33] trinuclear clusters receive extra stability from the σ-aromatic distribution of the six M–M bonding electrons. The factor does likely counterbalance the repulsive effect mentioned above.

Puckering of Square Clusters. Another geometrical feature common to clusters **1** and **2** is the nonperfect coplanarity of the square skeleton. Recall that cyclobutane itself is a nonplanar molecule with a small energy barrier for the puckering (ca. 1–2 kcal mol^{-1}).[34] The potential energy surface for carbonyl bonding to Os_4 in $Os_4(CO)_{16}$ has been calculated by Lauher[31] as a function of a distortion from D_{4h} symmetry and in any case the distortional barriers are low. By examining a three-dimensional model of $Os_4(CO)_{16}$ it becomes clear that the puckering of the tetranuclear skeleton is achieved through combined torsions about parallel Os–Os edges. The molecule's symmetry descends from D_{4h} to D_{2d}. The average torsion angle (τ) about M–M bonds (=0° in a planar skeleton) is as large as 15° in **2** and 10° in **1**. Also, the puckering can be described by the dihedral angle (δ) between two M_3 planes having in common the M_3–M_4 diagonal, see XVII.[35]

Notice that the D_{2d} symmetry requires an equal δ folding at the second diagonal (M_1–M_2). Another well-known class of tetranuclear clusters, i.e., butterflies with C_{2v} symmetry, is distinguishable from puckered-square clusters for having two different δ angles. The unique experimental δ value in **2** and **1** is 158.9° and 164.8°, respectively.

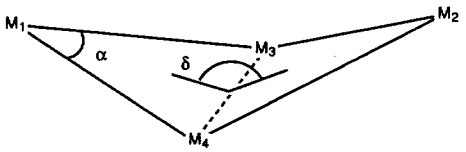

XVII

Also, δ correlates with bond angles M–M–M (α) according to the expression: $\sin(\alpha/2) = \tan(\delta/2)$. A δ puckering of 158° induces an insignificant α variation of only 1.0°, as experimentally found. The important point to be made is that the molecule has a great deal of freedom to fold without requiring rehybridization of the metal orbitals involved in the formation of metal–metal bonds. Hence, no geometric rearrangement of the ML_4 fragments takes place that may have some major electronic consequence. More likely the puckering can be due to packing and/or steric requirements, with a low-energy cost. The argument seems to have a general validity for any square ring, and also the well-known puckering of cyclobutane can be accounted for by considering that no change of the carbon hybrids directionality is required.

The above arguments are confirmed by the MO calculations. Even large δ variations have little consequences. The interactions involving the tangential orbitals (b_{1g}) are totally unaffected. A certain loss of overlap between the in-pointing radial orbitals, no longer directed toward the baricenter of the square, affects the HOMO $2a_{1g}$ (compare XIV with XVIII). Nonetheless the energy of the level as well as the total energy of the system is not significantly changed.

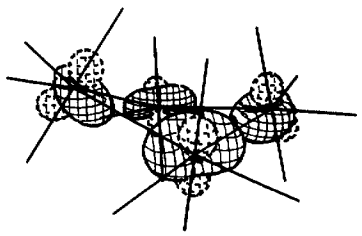

XVIII

$[Re_4(\mu_4\text{-}C)(CO)_{15}I]^-$, a Cluster Containing an Interstitial Carbide. The ease by which square compounds can pucker allows to include $[Re_4(\mu_4\text{-}C)(CO)_{15}I]^-$, **3**, shown in XIX, in the field of compounds to investigate.

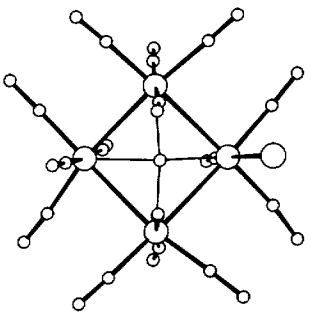

$[Re_4(\mu_4\text{-}C)(CO)_{15}I]^-$, **3**

XIX

All of the Re–Re bonds are similar [3.00 (1) Å (av)], but the angle δ (defined in XVII) is far from 180° [=137.7°]. Even so,

(33) (a) Mealli, C. *J. Am. Chem. Soc.* **1985**, *107*, 2245. (b) Mealli, C.; Proserpio, D. M. *Comments Inorg. Chem.* **1989**, *9*, 37.

(34) Cremer, D. *J. Am. Chem. Soc.* **1977**, *99*, 1307 and references therein.

(35) δ correlates with τ according to $[\sin(\delta/2)]^2 = \cos\tau$. See: Dunitz, J. D. *X-ray Analysis and the Structure of Organic Molecules*; Cornell University Press: Ithaca, NY, 1979; p 423. Experimental values of τ in compounds **1**, **2**, and **3** are slightly asymmetric, but their average coincides with the calculated value.

the α angles at each Re atom are only 4° less than 90°. The molecule can still be considered an inorganic cyclobutane with the peculiarity of an interstitial carbon atom at the center of the ring. Several M_4 carbide clusters are known,[36] but they all have a butterfly shape with one large puckering angle ($\delta < 120°$ and $\alpha < 70°$). In **3** the carbon atom is chemically unique because it is coordinated to another four atoms (the metals) in a quasi-planar environment.

Interstitial carbon atoms are considered to have no major role in fixing the geometry of clusters but supply their valence electrons to the system.[37] Still the carbon orbitals are engaged in bonding interactions with the metals. This is also seen from the MO analysis of **3**. The s, p_x, and p_y carbon orbitals have a_{1g} and e_u symmetries in D_{4h}. Essentially, they interact positively not only with three low-lying metal orbitals of M_4L_{16}, i.e., the lone pairs $1a_{1g}$ and $1e_u$ of Figure 1, but also with the higher $2a_{1g}$ and $2e_u$ levels. Since the latter have mainly M_4 bonding character, the intrusion of carbon stabilizes all the filled a_{1g} and e_u MOs (hence the whole system) but this occurs at the expense of the M–M bond strengths. In fact, the corresponding OP values are strongly reduced in the carbide with respect to the 64e⁻ carbon-free model.

Even if there are large mixings, $1a_{1g}/2a_{1g}$ and $1e_u/2e_u$, still the metal–carbon interactions can be seen as formal backdonations from three of the four M_4L_{16} lone pairs (the in-plane ones, shown in XVI). The fourth lone pair, $1b_{2g}$, does not have the right symmetry to interact with carbon p_z (a_{2u}). In any case the latter carbon orbital receives some backdonation from a combination of metal $d\pi_\perp$ orbitals. The antibonding partner corresponding to the latter interaction (shown in XX) is the LUMO.

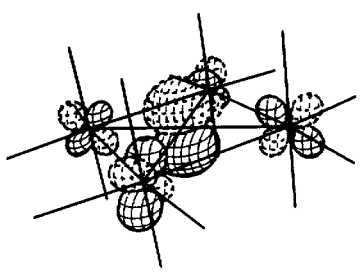

XX

The large carbon character of LUMO allows prediction of the residual carbon nucleophilicity, but unfortunately no experimental information on this type of reactivity is available. Analogously to the non-carbide M_4L_{16} clusters, the puckering of the square skeleton has no major energetic consequences. A Walsh diagram (not shown) indicates that all of the levels remain almost unperturbed along the distortional pathway. Perhaps the major effect of lowering the symmetry is the mixing of in-plane (σ) with out-of-plane ($d\pi_\perp$) metal lone pairs. Thus, the formerly unused $1b_{2g}$ lone pair is allowed to participate in backbonding to the carbon orbital p_z (a_{2u}) as both levels take the same b_2 symmetry (in D_{2d}). The population of p_z increases consequently (from 0.56 to 0.60 in the δ range 180°–135°). Although numerically small the effect can be an additional driving force to the molecular puckering.

62e⁻ Rhombus Clusters and Their Ideal Descent from 64e⁻ Conformers. In the rhombus $[Re_4(CO)_{16}]^{2-}$, **10** (see II), one diagonal is practically equal to the four sides (see Table I). It was postulated[7] that this 62e⁻ planar cluster descends from tetrahedral 60e⁻ clusters upon the addition of an electron pair to one M–M antibonding MO. The cleavage of one of the six tetrahedral edges would convert the species into the flat triangulated parallelogram of **10**, through butterfly intermediates.

We prefer to think of the rhombus as descending from the square $M_4(CO)_{16}$ species upon a two-electron oxidation. This implies a least motion pathway with minimum metal orbital

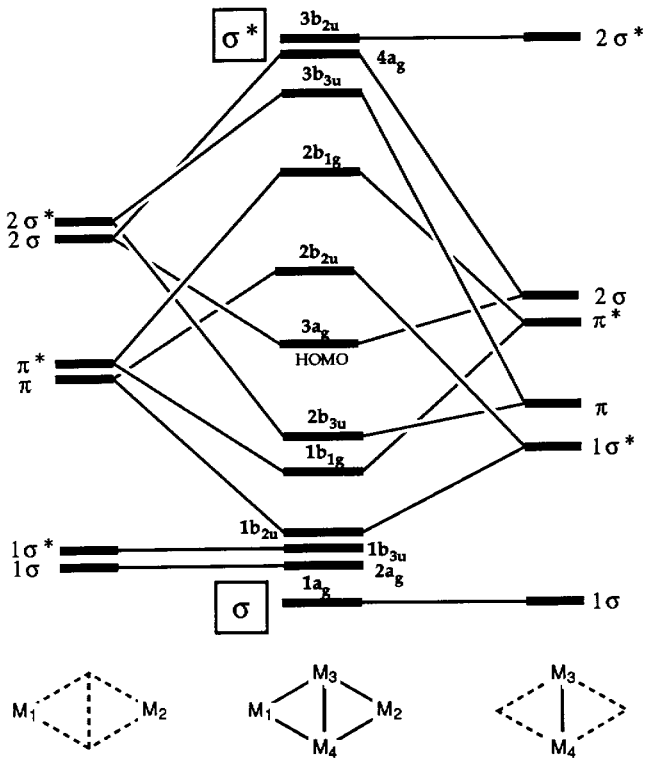

Figure 2. General diagram for the construction of the MOs of rhombus clusters of the type M_4L_{16} from pairs of orthogonally oriented $L_4M\cdots ML_4$ fragments.

rehybridization. Also, the correlations between electronic and orbital features can be envisaged from a unique viewpoint.

Figure 2, analogous to Figure 1, reports the diagram for the interaction between the FMOs of two orthogonally oriented $L_4M\cdots ML_4$ groupings. Now the right most fragment contains two metals already at a bonding distance. Accordingly, while the levels at the left side are essentially those of Figure **1**, the FMO levels on the right are more split σ/σ^* and π/π^* combinations. Due to the hybridization of the components, the largest gap is observed between the 2σ and $2\sigma^*$ components although $1\sigma^*$ is higher than before and lies closer to the almost degenerate π and π^* levels of the other fragment. The match between π and $1\sigma^*$ is highly favored. The antibonding partner of the latter $1\sigma^*/\pi$ interaction is pushed to an energy high enough for it to remain unpopulated ($2b_{2u}$ = LUMO). The level relates directly to one member of the bonding and filled $2e_u$ set, the second HOMO of square clusters (see XIII and Figure 1). Figure 3 shows the evolution of the MO levels and in particular that of $2b_{2u}$, along the $D_{4h} \rightarrow D_{2h}$ transformation pathway.

Three-dimensional orbital drawings illustrate the important change affecting the radial components of the vertical L_4M–ML_4 fragment. Initially there is a large sp character in them (see IX), but when $1\sigma^*$ mixes in, a torus-like contribution (z^2-type) is acquired and eventually this converts into the x^2–y^2 orbital type (see X). Along the pathway, the positive $2\sigma^*/\pi$ overlap first becomes null (a situation not dissimilar from XII), and then the π lobes of the horizontal metals interact in antibonding fashion with the out-pointing lobes of x^2–y^2 at the vertical metals. Eventually, $2b_{2u}$ lies sufficiently higher than the $3a_g$ level to favor a preferential 62e⁻ configuration with a rhombus geometry. The HOMO–LUMO gap is larger for $[Re_4(CO)_{16}]^{2-}$, (ca. 0.8 eV) than for the isoelectronic model $[Os_4(CO)_{16}]^{2+}$ (ca. 0.5 eV). If the $3a_g$ and $2b_{2u}$ levels are both occupied (64e⁻ configuration), the ring squeezing with crossing of the two levels implies no ground state change. Anyway, a higher total energy and the fact that $2b_{2u}$ is M_4 antibonding in character seem to exclude an easy access to the rhombus geometry.

Also, it would be interesting to know the electrochemical behavior of the M_4L_{16} species. Predictably, a 2e⁻ reduction of a 62e⁻ isomer should smoothly transform the rhombus into a square,

(36) Wijeyesekera, S. D.; Hoffmann, R. *Organometallics* **1984**, *3*, 949. Wijeyesekera, S. D.; Hoffmann, R.; Wilker, C. N. *Organometallics* **1984**, *3*, 962. Harris, S.; Bradley, J. S. *Organometallics* **1984**, *3*, 1086. Ceulemans, A. *J. Chem. Phys.* **1986**, *84*, 6442.

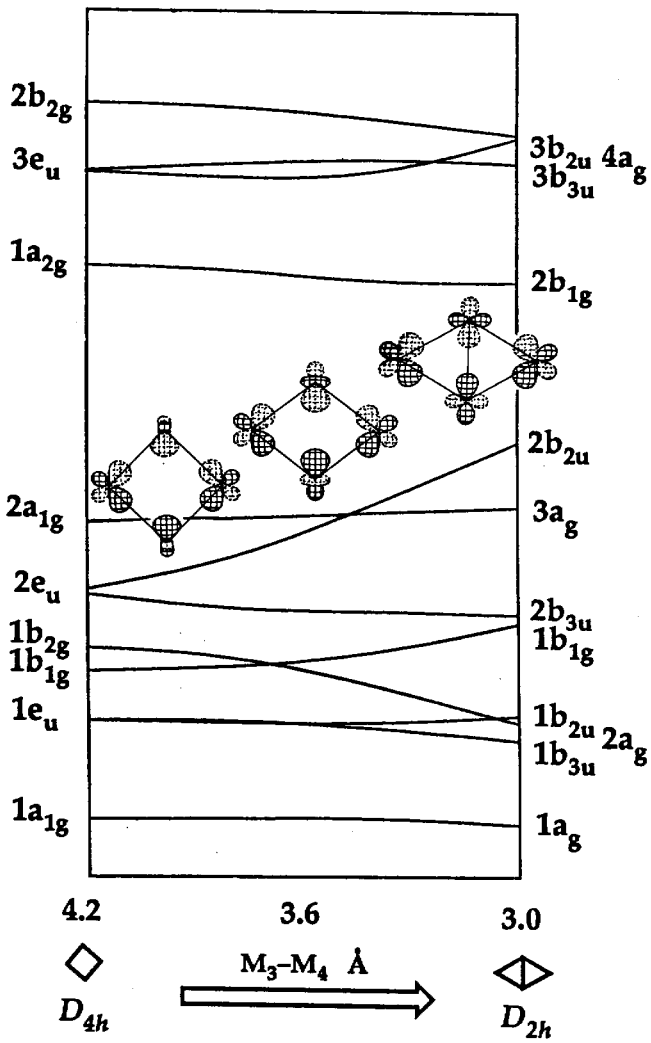

Figure 3. The correlation of the MOs of M_4L_{16} planar clusters along the least motion pathway relating square and rhombus geometries. Three-dimensional drawings of the frontier level $2b_{2u}$ along the pathway show how its M_4 bonding transforms gradually into a M_4 antibonding character. The electron count preferences of the square (64) and of the rhombus (62) are easily accounted for.

whereas the reverse oxidation of a square cluster is in principle complicated by orbital correlations associated with the crossing of the frontier levels of different symmetry. In fact, a high energy barrier may render the process forbidden in the sense of the Woodward–Hoffmann rules.[38] By contrast, the constantly small HOMO–LUMO gap does also suggest that an excited triplet state (TS) may be not out of reach. The forbiddenness/allowedness of diamond–square–diamond transformations in closo clusters of the main group as well as of transition metals has been also considered by other authors.[39]

In the rhombus, four definitely positive OP values between FMOs suggest that also in this case four outer M–M bonds are formed. Three bonds are due, as in the square, to the interactions: $\langle 2\sigma/2\sigma \rangle$, $\langle \pi^*/\pi^* \rangle$, and $\langle 2\sigma^*/\pi \rangle$. The fourth bond is now generated from the interaction $\langle \pi/1\sigma^* \rangle$ and not from the $\langle \pi/2\sigma^* \rangle$ one.

The origin of an additional transannular M–M bond, having OP similar to the other bonds, can be inferred from Figure 2. In fact, the rightmost level $1\sigma^*$ is engaged in cyclic interactions, while its bonding partner (1σ) is not. The reverse situation occurs for the FMOs 2σ and $2\sigma^*$, with the former engaged in cyclic bonding. Eventually, the MOs descending from the rightmost 1σ and $2\sigma^*$ FMOs are the pair of filled-bonding ($1a_g$)/empty-antibonding ($3b_{2u}$) orbitals that triggers the diagonal metal–metal bond.[40]

The $1\sigma/1\sigma^*$ pair, that originates the diagonal M–M bond, descends largely from the metal t_{2g} sets. In terms of isolobal analogy applied to ML_4 (C_{2v}) fragments,[29] t_{2g} orbitals are usually excluded from the number of frontier metal hybrids, or they are assigned bonding capabilities. If metal–ligand interactions alone are examined, we are aware of no example where a d^8-ML_4 fragment coordinates to three extra ligands, all lying in the equatorial plane and being 60° apart from each other. However, these are exactly the directions of the three M–M bonds departing from one ML_4 fragment in the rhombus cluster.

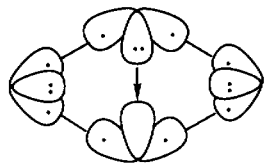

XXI

In the rhombus the $\pi/1\sigma^*$ antibonding combination ($2b_{2u}$) is empty. To make it simple, we can imagine that the two missing electrons mainly belonged to $1\sigma^*$, a former t_{2g} lone pair at one metal. This allows the metal in the trans diagonal site to use an equivalent t_{2g} pair and to trigger the new M–M bond, as shown in XXI (to compare with XVI). There remain ten lone pairs at the metals (eight $d\pi_\perp$ or $d\delta$ and two σ ones).

Before we close this section we mention two other $62e^-$ clusters, namely $Os_4(CO)_{12}(\mu\text{-}CF_3CO_2)_2$, **11**, and $Os_3ReH(CO)_{15}$, **12**, that closely resemble $[Re_4(CO)_{16}]^{2-}$, **10**. In **12** the five M–M bonds are remarkably similar to each other in spite of the heteronuclearity of the compound. By contrast, in **11** the chelate ligands buttress the structural distortion of the rhombus to a parallelogram as it is true that the two sides bridged by the acetato groups are ca. 0.1 Å shorter than the other pair of unbridged sides.

$62e^-$ M_4L_{15} Clusters. It has been pointed out above that $62e^-$ rhombuses can hardly derive from $64e^-$ squares upon a $2e^-$ oxidation on account of Woodward–Hoffmann rules.[38] By analogy, it is unlikely that a two-electron donor departs easily from $64e^-$ M_4L_{16} compounds. Indeed, $Os_4(CO)_{15}$, **13**, shown in XXII, is not reported to form from $Os_4(CO)_{16}$, **2**, upon the loss of a carbonyl ligand. On the contrary, **2** forms from **13** by addition of one CO ligand,[10] an allowed two-electron reduction of some sort.

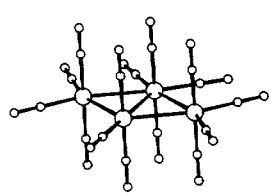

$Os_4(CO)_{15}$, **13**

XXII

In any event, we pursue an ideal continuity between 62 and $64e^-$ planar clusters. How different are the electronic features and the intermetal bonding network between the two $62e^-$ species, $M_4(CO)_{16}$ and $M_4(CO)_{15}$? The EAN rule predicts five M–M bonds in both cases so that the number of metal lone pairs must be different. Consider $M_4(CO)_{15}$ with a total of 36 metal orbitals available. Fifteen of these are used for metal–ligand interactions that involve 30 of the 62 electrons. There remain 21 orbitals and 32 electrons available. Eventually, the metal orbitals will be

(37) Minkin, V. I.; Minyaev, R. M.; Zhdanov, Yu. A. *Nonclassical Structures of Organic Compounds*; MIR: Moscow, 1987; Chapter 6.3.
(38) Woodward, R. B.; Hoffmann, R. *Angew. Chem., Int. Ed. Engl.* **1969**, *8*, 781.
(39) (a) Gimarc, B. M.; Ott, J. J. *Inorg. Chem.* **1986**, *25*, 2708. (b) Wales, D. J.; Stone, A. J. *Ibid.* **1987**, *26*, 3845. (c) Wales, D. J.; Mingos, D. M. P.; Zhenyang, L. *Ibid.* **1989**, *28*, 2754.

(40) A very similar symmetry argument[3] does account for the existence of a Fe–Fe bond in $Fe_2(CO)_9$ although, in that case, a calculated negative OP had previously convinced several authors to deny its existence. The latter numerical result is a consequence of a through-bond coupling that does not necessarily exclude a direct Fe–Fe σ interaction.

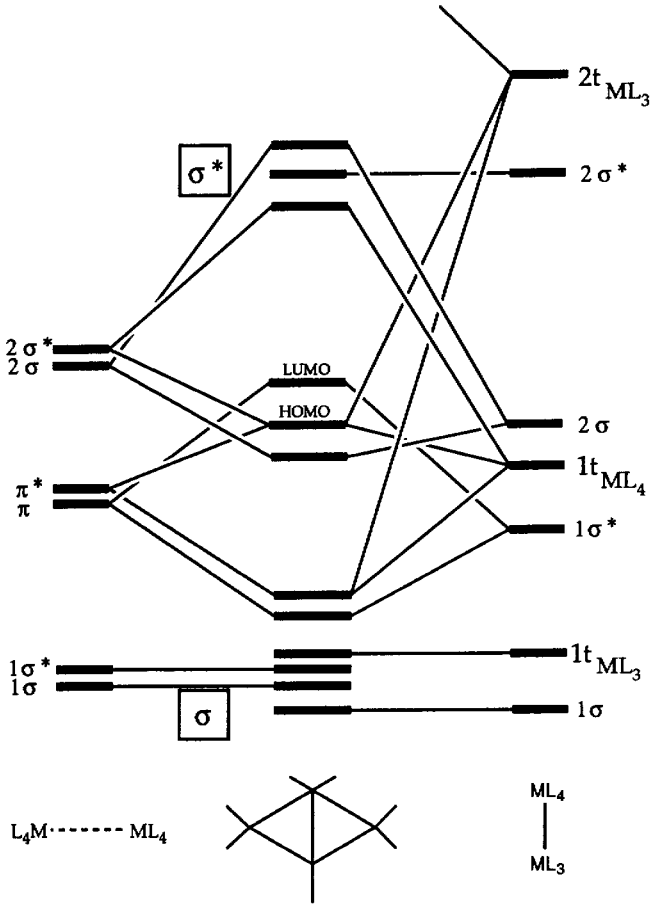

Figure 4. Diagram for the construction of the MOs of the rhombus cluster $Os_4(CO)_{15}$ from the orthogonally oriented $(CO)_4M\cdots M(CO)_4$ and $(CO)_4M-M(CO)_3$ fragments. Recall that each metal has two coordinated axial ligands that for the sake of clarity are omitted in the cluster's sketch.

distributed in m pairs of bonding and antibonding M–M levels and n lone pairs. Since only m (bonding) and n (lone pairs) will be doubly populated, the system of equations XXIII can be written.

$$2m + n = \text{no. of metal orbitals} \quad [=21 \text{ in } Os_4(CO)_{15}]$$

$$2m + 2n = \text{no. of metal electrons} \quad [=32 \text{ in } Os_4(CO)_{15}]$$

XXIII

The solution $m = 5$ and $n = 11$ confirms the expected five metal–metal bonds. When applied to $M_4(CO)_{16}$ compounds with 64 and 62 electrons, XXIII has solutions $m = 4$, $n = 12$ and $m = 5$, $n = 10$, respectively. The derived number of metal lone pairs (n) is an additional guideline to analyze the overall MO picture.

Eight out-of-plane lone pairs are common to all cases, whereas the four and the two σ-lone pairs in 64 and 62e⁻ $M_4(CO)_{16}$ compounds have been depicted in XVI and XXI and discussed. For $M_4(CO)_{15}$ the expected three σ-lone pairs and the five bonding/antibonding MO partners need to be identified in the overall MO picture (vide infra).

Bonding Os–Os distances in **13** can be as different as >0.2 Å (see Table I). Analogous trends are observed in compounds **14** and **15** that have the primary M_4L_{15} composition but with different ligands (phosphine or cyclopentadienyl substituting for some carbonyls) and/or a M_4 heteronuclear skeleton (**15**). The question is raised whether all of the Os–Os linkages continue to have bond order one.

Before proceeding any further, we mention that the Os–Os OP values, calculated for a model of **13**, are quite consistent with the experimental trends. In fact, the shortest sides, connecting the unique T-shaped ML_3 fragment with the two adjacent ML_4 fragments, have a length of 2.772 (1) Å and an OP value of 0.204. The other two sides of the quadrilateral have experimental and calculated magnitudes of 2.997 (1) Å and 0.155, respectively. Finally the diagonal is intermediate at both experimental and computational levels (2.948 (1) Å and 0.186, respectively). The numerical results are not biased by the use of different Os–Os distances (all fixed at 2.9 Å). Essentially, the EHMO method is suited to extract reliable semiquantitative information.

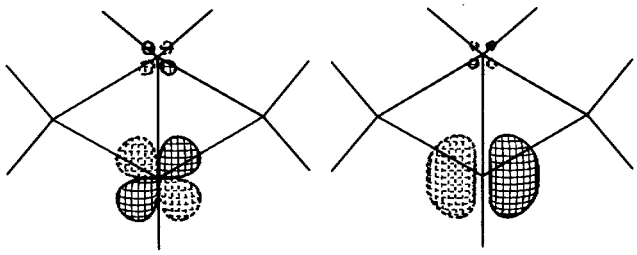

XXIV XXV

Again, the bonding is analyzed by sectioning $Os_4(CO)_{15}$ into two parts: on the left side of Figure 4, the horizontal $L_4M\cdots ML_4$ grouping and, on the right side, the vertical L_3M-ML_4 one. The reader should not forget that, although omitted from most of the in-plane projections (Figure 4 and XXIV–XXVII), there are pairs of axial ligands coordinated to all of the metals.

There is an important difference with respect to the rhombus of Figure 2. The lack of one equatorial ligand at one metal leaves an extra π tangential orbital available for σ-bonding. In summary, the two π and π^* combinations, equally distributed in $L_4M\cdots ML_4$, become localized each at a different metals in L_3M-ML_4. These are indicated as $1t_{ML_3}$ (pure d, XXIV) and $1t_{ML_4}$ (as in XI) to which the high-lying, $2t_{ML_3}$ level (pure p, XXV) is added.

The lack of mirror symmetry in L_3M-ML_4 allows a lot of orbital mixing. However, the knowledge of square and rhombus models now becomes important. Essentially, the 2σ, $2\sigma^*$, π, and π^* combinations of the L_4M-ML_4 grouping (1σ and $1\sigma^*$ remain as lone pairs) match the FMOs 2σ, $1t_{ML_4}$, $1\sigma^*$, and $2t_{ML_3}$ of the other fragment, in order to make cyclic bonds. Unmatched 1σ and $2\sigma^*$, filled and empty MOs respectively, justify one trans diagonal M–M linkage.

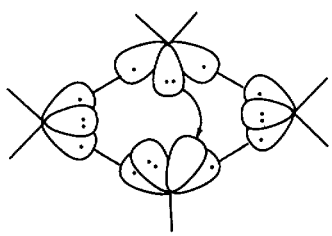

XXVI

Finally, $1t_{ML_3}$ is unused and, being filled it represents the 11th lone pair of the system. Similar to the schemes XVI and XXI, XXVI illustrates where the three σ lone pairs are localized on and where the trans diagonal bond originates from. Since the bonding MO (1σ) has a smaller percentage of ML_3 character, the electron flow along the diagonal appears as a donation from ML_4 to ML_3.

The nonequivalence of the M–M interactions, hence the relative bond strengths, must be associated with the three different metal environments and correspondingly different hybridizations. Obviously the M–M OP cannot be the same in all of the bonding directions. Still, the number of metal orbitals involved is appropriate for having the equivalent of five distinguished two-center/two-electron bonds in the cluster. Other conclusions,[25] based on different (fractional) M–M bond orders, seem less probable in light of the present analysis. For example, bond orders of 1.5 imply a percentage of M–M double bonding of which we find no trace.

As for other 62e⁻ species, the HOMO–LUMO gap is small but somewhat dependent on the model. For example, the use of the most complete all-carbonyl model provides a sufficiently large ΔE (ca. 0.8 eV). The composition of LUMO is quite similar to that found for the $Os_4(CO)_{16}$ rhombus (see $2b_{2u}$ at the right side of Figure 3). By contrast the HOMO (XXVII) is a complex mixture of π^*, $2\sigma^*$ (from $L_4M\cdots ML_4$) and of $1t_{ML_4}$, $2t_{ML_3}$ (from $L_3M\cdots ML_4$).

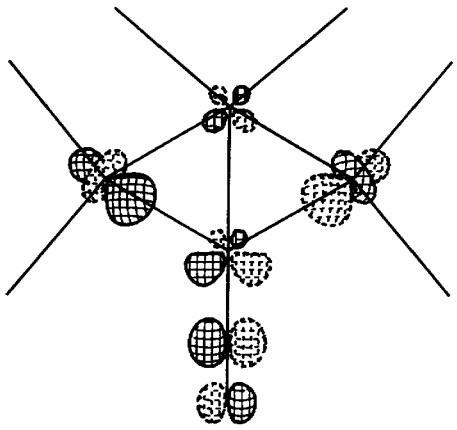

XXVII

As a simplification based on the nodal properties and on the values of the OP between FMOs, the latter level can be imagined as resulting from canonical $\langle\pi^*/\pi^*\rangle$ cyclic interaction (b_{1g} in VII), which is able to provide one fourth of the M_4 bonding. Notice that the ML_3 plane is nodal for the HOMO, but the two intermetal regions, connecting $Os(CO)_3$ with the two adjacent fragments and extended to the carbonyl carbon atom, are not noded. First, the feature suggests that the two Os–Os bonds departing from $Os(CO)_3$ are well localized, hence stronger. Then, it is reasonable to assume that an electrophile is preferentially attracted by the electron density of the HOMO, largely distributed at the two consecutive Os–Os bonds. The point is not necessarily in contrast with the fact that the system takes up another CO ligand to give $Os_4(CO)_{16}$.

Cluster with Coplanar Phosphide Bridges. Recently Carty et al.[13] have reported the characterization of two tetranuclear 64e⁻ ruthenium clusters $Ru_4(CO)_{13}(\mu\text{-}PPh_2)_2$, **7**, and $Ru_4(CO)_{10}(\mu\text{-}PPh_2)_4$, **6** (shown in III and IV, respectively). All of the metals are coordinated by pairs of axial CO ligands, but the two compounds differ for having two or four Ru–Ru sides bridged by phosphido groups. Also, the numbers of equatorial CO ligands per metal are different in the two cases, being 2,1,1,1 in **7** and 2,0,2,0 in **6**, respectively.

The EAN rule predicts the existence of four single M–M bonds in both compounds, but the M_4 ring is in no case a square. In addition, by counting the number of metal–ligand bonds and by applying equations of type XXIII, the existence of 11 and 10 metal lone pairs is expected for **7** and **6**, respectively.

The metal skeleton in **7** is essentially formed by two condensed triangles having in common one side (the short quadrilateral's diagonal) of 3.1335 (4) Å. The two PPh_2-bridged sides are longer [av = 3.17 (2) Å], while the unbridged sides are the shortest Ru–Ru vectors [av = 2.91 (1) Å]. This trend is also observed in the compounds **9** and **8** (see Table I). While the former is an heteronuclear analogue of **7** (one Fe in place of one Ru atom), **8** differs from **7** in the replacement of one phosphido bridge with an acetylide (see XXVIII). In the specific bridging mode the acetylide acts also as a four-electron donor.

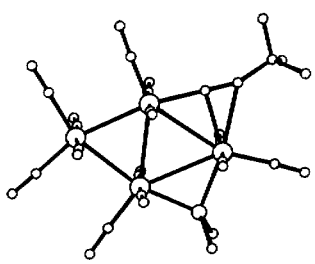

$Ru_4(CO)_{13}(\mu\text{-}PPh_2)(\mu\text{-}\eta^2\text{-}C{\equiv}C\text{-}t\text{-}Bu)$, **8**

XXVIII

By neglecting the out-of-plane CO ligands and by taking the unique $Ru(CO)_4$ fragment as a simple 4e⁻ donor bridge, the rightmost triangle of **7** and **8** may be compared with that found in some triangular clusters of the type $M_3L_3(\mu\text{-}L')_3$ (M = Pd, Pt; L' = π-donor), e.g., $Pd_3L_3(\mu\text{-}PPh_2)_2(\mu\text{-}Cl)$[41] and $Pt_3L_3(\mu\text{-}PPh_2)_3$.[42] Already, we found the idea of the interchangeability between π-donor bridges, such as phosphido, and L_4M fragments (M = Fe, Ru) to work well in polynuclear two-dimensional clusters.[33a]

Recently, we have noticed[43] a strict analogy between the above-mentioned 44e⁻ trinuclear clusters and the 86e⁻ hexanuclear planar cluster $[Fe_3Pt_3(CO)_{15}]^{2-}$ in which three (CO)Pt fragments are connected by three $(CO)_4Fe$ bridges.[44]

In all of the previous compounds, the inner M–M triangular sides have bond orders of 2/3. In fact, it is commonly found that all of the possible combinations of radial and tangential FMOs distribute as three bonding below three antibonding MOs, as shown in XXIX. When there are only 42 electrons available, as in clusters with π-acceptor bridges [e.g., $(CNR)_3Pt_3(\mu\text{-}CNR)_3$[45]], the filling of the MOs XXIX is of the σ-aromatic type,[46] and there are three single M–M bonds. An additional electron pair in the level $\sigma(t)^*$ either destroys one M–M bond or weakens the overall M_3 bond strength in the equilateral triangle.

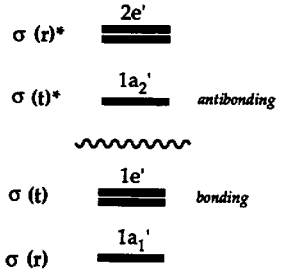

XXIX

The dichotomy is beautifully exhibited by a particular crystallization of the cluster $Pt_3Ph(PPh_3)_2(\mu\text{-}PPh_2)_3$.[42b] that contains both types of conformers in the asymmetric unit. Evidence that $\sigma(t)^*$ is the HOMO for all of the comparable systems of this type is provided by the redox chemistry of $[Fe_3Pt_3(CO)_{15}]^{2-}$.[43] Both 85 and 84e⁻ derivatives are obtainable (via chemistry or electrochemistry), and the experimental structures[42b,47] confirm the progressive increase of the Pt–Pt bond order from 2/3 to 1.

Ru–Ru bond orders of 2/3 seem appropriate also for the rightmost triangle of clusters **7**–**9**. The FMO analysis shows that two single Ru–Ru bonds depart from the unique $Ru(CO)_4$ fragment. The corresponding interaction diagram is not shown in detail, but essentially there are two strong interactions of σ and π type between the well-known frontier orbitals of the fragment ML_4 (C_{2v} symmetry) with two properly oriented hybrids of the fragment $Ru_3(CO)_9(\mu\text{-}PPh_2)_2$ (XXX). Also, due to the relative energies of the interacting orbitals, the assumption that a fragment $[Ru(CO)_4]^{2-}$ (d^{10}) substitutes for a third bridging phosphido ligand appears reasonable.

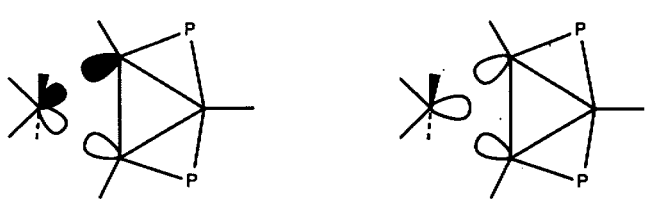

XXX

(41) Bushnell, G. W.; Dixon, K. R.; Moroney, P. M.; Ratay, A. D.; Wan, C. *J. Chem. Soc., Chem. Commun.* **1977**, 709.
(42) (a) Taylor, N. J.; Chieh, P.; Carty, A. J. *J. Chem. Soc., Chem. Commun.* **1975**, 448. (b) Bender, R.; Braunstein, P.; Tiripicchio, A.; Tiripicchio-Camellini, M. *Angew. Chem., Int. Ed. Engl.* **1985**, *24*, 861.
(43) Della Pergola, R.; Garlaschelli, L.; Mealli, C.; Proserpio, D. M.; Zanello, P. *J. Cluster Science* **1990**, *1*, 000.
(44) Longoni, G.; Manassero, M.; Sansoni, M. *J. Am. Chem. Soc.* **1980**, *102*, 7974.
(45) Bushnell, G. W.; Dixon, K. R.; Moroney, P. M.; Ratay, A. D.; Wan, C. *J. Chem. Soc., Chem. Commun.* **1977**, 709.
(46) Dewar, M. J. S. *J. Am. Chem. Soc.* **1984**, *106*, 669.
(47) Adams, R. D.; Chen, G.; Wang, J.-G. *Polyhedron* **1989**, *8*, 2521.

Chart II

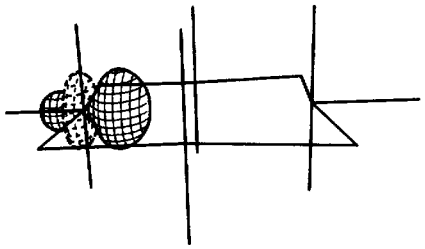

XXXIV

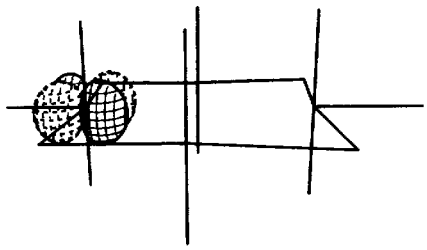

XXXV

The interaction with $[Ru(CO)_4]^{2-}$ does not change the σ-MO pattern (of the type XXIX) inside of the fragment $[Ru_3(CO)_9(\mu\text{-}PPh_2)_2]^{2+}$. Since the HOMO is again of the $\sigma(t)^*$ type, the third and fourth Ru–Ru bonds are delocalized over the three sides of the rightmost triangle. An increasing deformation of the equilateral shape (shortening of the shared side), found in compounds **7**, **8**, and **9**, can be attributable to the increased number of different bridges and to the heteronuclearity of the system (cluster **9**). In any case, the computed OP values follow the experimental trends (see Table I).

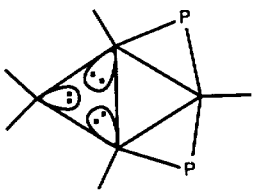

XXXI

Finally, it is also possible to identify the three in-plane metal lone pairs besides those eight having $d\pi_\perp$ or $d\delta$ character. As shown in XXXI, they all point toward the center of the leftmost triangle, as each one identifies with a "t_{2g}" member of a ML_4 fragment, similarly to the $Os_3(CO)_{12}$ case.

The electronic features of cluster **6**, shown in IV, are even more challenging, but again a good agreement between the computed Ru–Ru OP and the experimental bond lengths suggests that the EHMO method tackles the problems adequately. How correct is the EAN rule in predicting a total of four single Ru–Ru bonds in **6** and how are they eventually distributed?

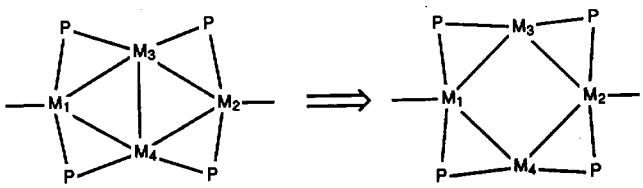

XXXII XXXIII

One ring diagonal [M_3–M_4 = 2.8355 (7) Å] is the shortest, and all four sides are equally long [3.05 (1) Å]. The Ru_4 skeleton, a rhombus (XXXII) rather than a square (XXXIII), could suggest a close similarity with the series of 62e$^-$ derivatives, but there are not five metal–metal bonds. Besides, the following arguments show that even the square model XXXIII, with four outer σ M–M bonds, is not electronically feasible.

In the square skeleton, the M_3 and M_4 atoms are almost square planarly coordinated by ligands, whereas the lateral ML_5 fragments are square pyramidal (these considerations are made on the basis that each phosphido group is the equivalent of two overlapping terminal ligands).

A square planar d^8 metal is electronically saturated with the p_z orbital unavailable either for bonding or lone pairs. As a consequence, the total number of metal orbitals in XXXIII would be 34 rather than 36 (=4 × 9), and the EAN rule would predict two M–M bonds at most.

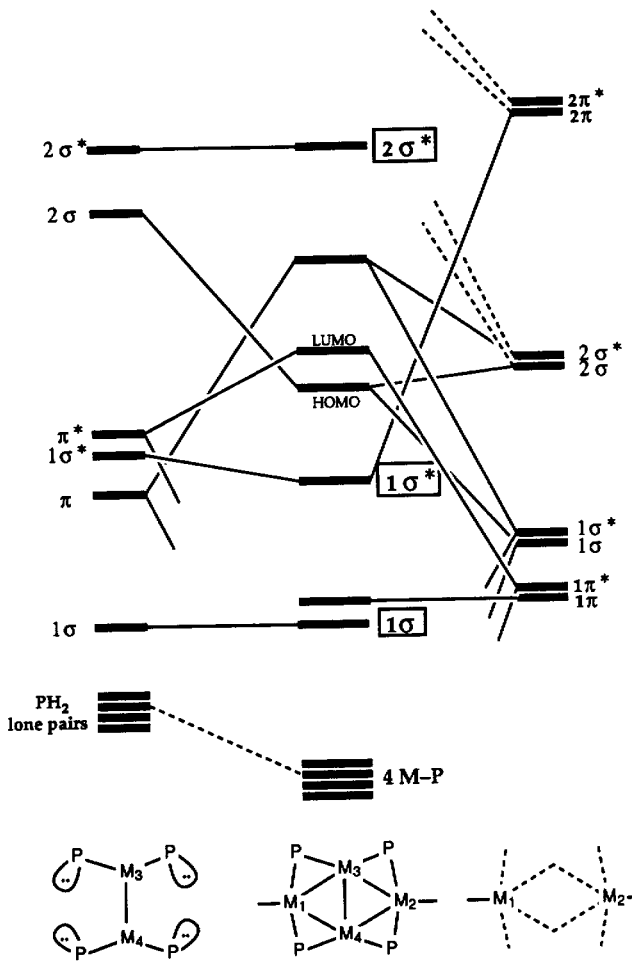

Figure 5. Interaction diagram for the formation of $Ru_4(CO)_{10}(\mu\text{-}PPh_2)_4$ from fragments. Dashed lines indicate the origin of the bonding and antibonding Ru–P molecular orbitals. Although a large rehybridization occurs in the right side between 1σ and 2σ as well as between $1\sigma^*$ and $2\sigma^*$, the contributions to the MOs are kept separated for the sake of clarity. Also, notice that two axial ligands per metal are omitted from the cluster's sketch.

In order to construct an outer σ-bonding scheme of type VII, the two d^6 ML_5 fragments can provide empty σ hybrids (XXXIV) and filled pure d_π orbitals (XXXV). This is the type of isolobal analogy predicted by Hoffmann to involve t_{2g} metal orbitals.[1] The square ML_4 units have d_{z^2} (radial) and d_{xz} (tangential) orbitals, both filled. In any event, a total of 12 electrons in eight MOs is inconsistent with the presence of four metal–metal bonds. Nor the system appears characterized by two bonds over the four centers.

Experimentally, the ML_4 centers (M_3 and M_4) conform to a nonplanar C_{2v} geometry (butterfly fragments). This rehybridizes the radial p_z orbitals and makes them available for bonding. Since the ML_5 fragments are not changed, the interplay concerns now 10 orbitals and 12 electrons. We must have in mind the latter standpoint in analyzing the results from MO calculations.

Chart III

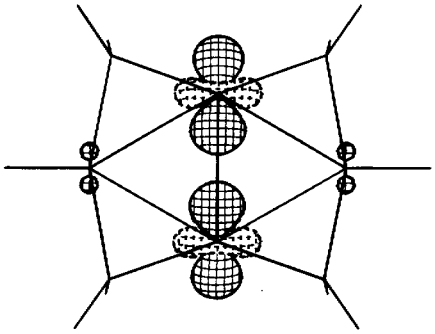

XXXVI

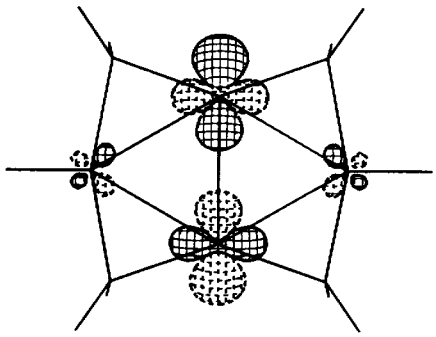

XXXVII

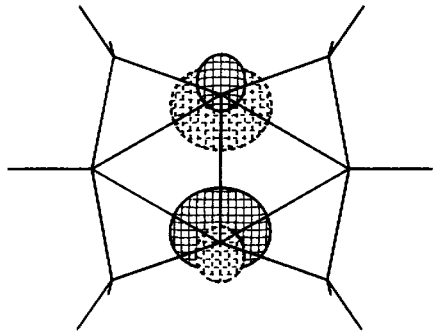

XXXVIII

In the FMO analysis of the model sketched in XXXII it is impossible to exploit directly the knowledge of familiar ML_4 and ML_5 frontier orbitals because the phosphido bridges cannot be split into halves. Thus, we chose a fragmentation where pairs of $RuL_2(PH_2)_2$ and T-shaped RuL_3 fragments[48] interact together. The relative interaction diagram (Figure 5) contains not only information on the Ru–Ru bonds but also that on the four Ru–P bonds being formed.

There are four symmetry combinations of filled phosphorus orbitals in the low left side of Figure 5. These lone pairs push up (dashed lines) four orbitals of the $L_3Ru\cdots RuL_3$ fragment, i.e., 2π, $2\pi^*$, σ, σ^*. While the π-type FMOs are combinations of metal p_y orbitals, those of σ-type are mixtures of the levels 1σ, 2σ and $1\sigma^*$, $2\sigma^*$ derived from the x^2-y^2 and p_x orbitals. For the sake of clarity in Figure 5 only 2σ, $2\sigma^*$ appear involved in Ru–P bonding. Thus, there remains a pair of σ and σ^* FMOs (formally, the still empty 1σ and $1\sigma^*$ ones) available for metal–metal interactions. The low filled 1π and $1\pi^*$ set (xy) is also available.

Three Ru–Ru cyclic linkages are inferred by the large OP values of 0.27, 0.29, and 0.27 calculated for the interactions $\langle 2\sigma/1\sigma\rangle$, $\langle \pi/1\sigma^*\rangle$, and $\langle \pi^*/1\pi^*\rangle$, respectively. The antibonding MO corresponding to the $\langle \pi^*/1\pi^*\rangle$ interaction is destabilized and empty (LUMO). An interaction of the type $\langle \sigma^*/\pi\rangle$ would also be necessary to have a fourth Ru_4 cyclic bond, or the Ru–Ru bond order is only 3/4. The possible interaction between the FMOs $1\sigma^*$ and 1π is four-electron repulsive, and, in first approximation, the two levels (sixth and seventh from the bottom) represent two of the ten expected lone pairs (apply equation XXIII).

In actuality, the role of $1\sigma^*$ is crucial being more than an antibonding (or even nonbonding) combination of M_3 and M_4 radial orbitals. The calculation shows that $1\sigma^*$ has a residual positive interaction (OP = 0.11) with the high-lying 2π level of the rightmost fragment. Recall that the latter FMO 2π is already engaged in Ru–P bonding so that the additional interaction with $1\sigma^*$ lessens in turn the strength of some Ru–P linkages. This is also supported by experimental evidence (vide infra).

Still, the role of $1\sigma^*$ needs to be further analyzed. The interaction between the M_3 and M_4 atoms is characterized by the presence of two σ^* levels, one empty ($2\sigma^*$) and one filled ($1\sigma^*$). Among the in-phase FMOs, 2σ is engaged in M_4 bonding, while 1σ is not.

The configuration $(1\sigma)^2$, $(1\sigma^*)^2$, $(2\sigma^*)^0$, defined by the boxed MOs in Figure 5, allows the formulation of the idea of an atypical transannular Ru–Ru bond. Notice that the relevant MOs (XXXVI–XXXVIII) are largely centered on the M_3 and M_4 atoms. Single bonds are normally the result of a two-orbital/two-electron interaction involving filled σ and empty σ^* MOs. Here, the presence of the intermediate $1\sigma^*$ filled level, somewhat M_3–M_4 antibonding, mitigates but does not diminish the strength of the bond. This situation, describable as a three-orbital/four-electron bond, seems typical for polymetallic systems as we have encountered it in some hydride bridged transition-metal dimers of formula $L_3Rh(\mu\text{-}H)_3RhL_3$[49] with a somewhat elongated Rh–Rh bond.

Finally it should not be forgotten that the level $1\sigma^*$ is also engaged in a positive Ru_4 cyclic interaction with the combination 2π of the fragment $L_3Ru\cdots RuL_3$. The presence of 2π (partly rehybridized) can also be seen in XXXVII. Since part of the $1\sigma^*$ electron density is diverged into Ru–P antibonding levels, also the repulsion between the Ru_3 and Ru_4 atoms is mitigated. In other words, the atypicity of the Ru–Ru transannular bond is in part disappearing at the expense of the Ru–P bonds. It has been experimentally observed in **6** that the four vectors connecting the P atoms to the Ru_1 and Ru_2 atoms are ca. >0.1 Å longer the other four Ru–P vectors [2.286 (4) vs 2.388 (2) Å]. The corresponding OP values follow this trend.

To summarize, the overall in-plane bonding network in **6** (i.e., extended to Ru–P bonds) appears intermediate between two limiting descriptions.

First, $1\sigma^*$, centered at the M_3 and M_4 atoms, has little involvement in bonding (a pseudo lone pair). There would be eight equivalent Ru–P bridge-bonds, three cyclic Ru–Ru bonds (bond order = 3/4), and one atypical three-orbital/four-electron transannular linkage. The viewpoint is partially consistent with the EAN prediction of four M–M bonds and ten lone pairs (equation XXIII).

The other limiting viewpoint assumes that $1\sigma^*$ totally interacts with the 2π FMO of the M_1–M_2 fragment. In this case, there would be only seven M–P bonds and five M–M linkages of bond order 1. Notice that the description subtracts two electrons of the phosphorus atoms from the bonding network. The cluster's electron count decreases to 62, for which a rhombus skeleton is predicted.

The MO analysis shows that the actual situation is intermediate between the two limits described above. This result is hardly attainable by other approaches of empirical nature.

Before closing this section, we remark on the crucial importance of the P atoms that can even be considered part of the cluster framework. On this basis, one referee has suggested a strict analogy between the bisphosphido cluster **7** and other known M_6 clusters of similar planar triangular geometry, e.g., the $92e^-$ anion $[Ru_6H(\mu\text{-}O{=}CNMe_2)_2(\mu\text{-}CO)_4(CO)_{14}]^-$.[50] The suggestion is attractive for future developments.

Other 64 and 60 Electrons Tetranuclear Clusters with Reduced Intermetal Bonding Network. As mentioned in the introduction, there are examples of two-dimensional clusters in which the M_4 skeletal structure seems buttressed by the connectivity requirements of the bridging ligands and not by direct metal–metal interactions. The known examples are characterized by the square-planar coordination of the ligands about each metal. Under these circumstances, electron saturation of the metals is achieved with only 16 electrons so that there may be less of a need to activate metal–metal bonds. This is especially true for $64e^-$ species

(48) A description of the FMOs in the T-shaped L_3M fragments can be found at p 352 of ref 29.

(49) Bianchini, C.; Laschi, F.; Masi, D.; Mealli, C.; Meli, A.; Ottaviani, F. M.; Proserpio, D. M.; Sabat, M.; Zanello, P. *Inorg. Chem.* **1989**, *28*, 2552.

(50) Boag, N. M.; Knobler, C. B.; Kaesz, H. *Angew. Chem., Int. Ed. Engl.* **1983**, *2*, 249.

(64 = 16 × 4) such as $Ni_4(\mu\text{-SR})_8$, **4** (see V), a square with long Ni···Ni sides of 2.685 (6) Å. Also the isoelectronic cluster $Pd_4(\mu\text{-}CCl_3CO_2)_4(\mu\text{-}t\text{-}BuOO)_4$, **5** (see IXL), has four coplanar metal atoms but long Pd···Pd separations [2.917 (7) Å].

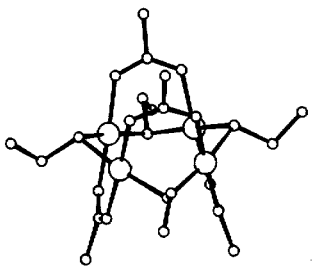

$Pd_4(\mu\text{-}CCl_3CO_2)_4(\mu\text{-}t\text{-}BuOO)_4$, **5**

IXL

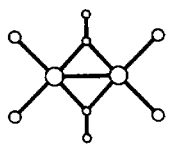

$[Pd_2Cl_4(\mu\text{-}CO)_2]^{2-}$

XL

More interesting is $Pd_4(\mu\text{-}CO)_4(\mu\text{-}CH_3CO_2)_4$, **16** (see VI), that has only 60 electrons. Two short (2.663 (1) Å) and two long (2.909 (1) Å) Pd–Pd sides and Pd–Pd–Pd angles of ca. 90° ± 7° define a parallelogram for the Pd_4 ring. The short sides are doubly bridged by two CO ligands, whereas the long ones are doubly bridged by two acetate chelates, each one providing two independent oxygen donors to adjacent metals. Essentially, the compound results from the assembly of two parallel dimers similar to the type characterized in the structure of $[Pd_2Cl_4(\mu\text{-}CO)_2]^{2-}$,[51] (see XL). Other isolated dimeric units of the type $M_2L_4(\mu\text{-}L')_2$ are known with L′ = π-donor, e.g., $Rh_2(CO)_4(\mu\text{-}PPh_2)_2$[52] and $Pd_2(CO)_2Cl_2(\mu\text{-}Cl)_2$.[53] In particular the latter compound (spectroscopically characterized) has the same composition of XL but with two less electrons (d^8 vs d^9 metals) and no Pd–Pd bond. Theoretical investigations have been performed by several authors,[54] but the nature of the Pd–Pd bond in XL presents some analogies with the problem of the Fe–Fe bond in $Fe_2(CO)_9$[3] as will be reported elsewhere.[55] Accordingly, two single and independent Pd–Pd bonds can be also hypothesized in the tetramer **16**. This is in agreement with the EAN rule considering that each metal has only eight atomic orbitals available.

Concerning the residual Pd–Pd interaction at the long sides of the parallelogram, it is well-known that d^8 square-planar monomers can pile up along the *z* direction through the formation of weak M–M bonds. The existence of filled d_{z^2} and empty p_z orbitals confers amphoteric character to the metals and allows a synergistic, doubly directional, donor–acceptor interaction. Analogously, the significant overlap of the d_{z^2} and p_z bands is at the origin of the polymeric one-dimensional stacking of $[Pt(CN)_4]^{2-}$ monomers.[56] In **16**, the stacking of the two dimeric units (as XL) is forced by the bridging acetate ligands, but there may also be a direct metal–metal bond. In no case can the latter be strong since the Pd–Pd vectors are not collinear with the normal PdL_4 planes (recall in fact that the Pd_4 ring is not a square but a parallelogram).

Conclusions

This study has examined in detail the M–M bonding features of the known tetranuclear two-dimensional clusters. The idea that the M_4 rings can be the analogues of the cyclobutane C_4 ring by virtue of the isolobal analogy is too simplistic. In fact, the availability of nine atomic orbitals makes the metals different from nontransition elements. In a new perspective, we have noticed that t_{2g} orbitals can participate in the formation of bonds in a way other than that predicted by special cases of the isolobal analogy.[1]

Table II. Atomic Parameters Used in the Calculations

atom	orbital	H_{ii} (eV)	ζ_1	ζ_2	C_1[a]	C_2[a]	refs
Os	6s	−8.17	2.45				57
	6p	−4.81	2.43				
	5d	−11.84	5.57	2.42	0.63684	0.55948	
Re	6s	−9.36	2.40				58
	6p	−5.96	2.37				
	5d	−12.66	5.34	2.28	0.63555	0.56738	
Ru	5s	−8.00	2.08				59
	5p	−4.30	2.04				
	4d	−12.20	4.21	1.95	0.57720	0.56920	
Pd	5s	−7.32	2.19				60
	5p	−3.75	2.15				
	4d	−12.02	5.98	2.61	0.52653	0.63745	
Ni	4s	−8.86	2.10				61
	4p	−4.90	2.10				
	3d	−12.99	5.75	2.00	0.56830	0.62920	
P	3s	−18.6	1.60				58
	3p	−14.0	1.60				
O	2s	−32.3	2.275				58
	2p	−14.8	2.275				
C	2s	−21.4	1.625				58
	2p	−11.4	1.625				
H	1s	−13.6	1.30				58

[a] Coefficients in double-ζ expansion.

The new bonding capabilities attributed to the metals account for the many overall bonding modes found in M_4 assemblies, and hopefully some of the models can be extended to bulk metals. Three coplanar M–M bonds at ca. 60° from each other, as found in $62e^-$ rhombuses, are the first evidence of the specificity of the M_4 network. In clusters of the type M_4L_{16}, the transition from 64 to $62e^-$ species and the attainment of a transannular bond is not a concerted process, but it can be framed in terms of a conceptual continuity that need not define two distinct categories of compounds (D_{4h} and D_{2h}).

It has been shown that the total electron count is not sufficient by itself to predict whether the distribution of the M–M bonds is only along the quadrilateral's perimeter or it involves a transannular direction as well. This becomes evident for the $64e^-$ clusters with phosphido bridges (**6**–**10**). The EAN rule prediction, that there are invariably four M–M bonds, may be incorrect, and in any case it cannot describe their distribution. The MO approach shows its superior interpretational power as it allows one to see the genesis of the bonds, how they are distributed, and whether they are fractional or not. A quite interesting case is that of cluster **6** in which a M–M bond is formed in part at expenses of some M–P bridge bonding. The fractional bond order for some of the M–M bonds is another good hint that an M_4 assembly may already contain features of the bulk metals.

Finally, the compounds studied, among the most simple in the realm of clusters, present a variety of different and complicated situations. No electron-counting scheme seems so general to adapt successfully to all of the cases. MO studies, aimed to establish the role of the different levels in the bonding network, provide the widest attainable information. The larger the molecules, the more difficult is the MO analysis, but the basic principles of orbital interactions maintain their own validity.

Computational Details

All of the MO calculations were of the extended Hückel type,[26] and a modified version of the Wolfsberg–Helmholz formula was used. The atomic parameters used[57-61] are summarized in Table II. The models used have the following general features: in the models with hydride ligands M–H = 1.7 Å, Re–Re = Os–Os = 2.9 Å, Ru–Ru = 3.0 Å, H–M–H (equatorial) 100°, H–M–H (axial) 180°; in the models with CO ligands M–C = 1.9 Å, C–O = 1.16 Å, C–M–C (equatorial) 100°,

(51) Goggin, P.; Goodfellow, R. J.; Herbert, I. R.; Orpen, A. G. *J. Chem. Soc., Chem. Commun.* **1981**, 1077.
(52) (a) Jones, R. A.; Wright, T. C.; Atwood, J. L.; Hunter, W. E. *Organometallics* **1983**, *2*, 470. (b) Jones, R. A.; Wright, T. C. *Ibid.* **1983**, *2*, 1842.
(53) Calderazzo, F.; Dell'Amico, D. R. *Inorg. Chem.* **1981**, *20*, 1310.
(54) (a) Kostic, N. M.; Fenske, R. F. *Inorg. Chem.* **1983**, *22*, 666. (b) Kang, S.-K.; Albright, T. A.; Wright, T. C.; Jones, R. A. *Organometallics* **1985**, *4*, 666.
(55) Mealli, C.; Proserpio, D. M. To be submitted for publication.
(56) Whangbo, M.-H.; Hoffmann, R. *J. Am. Chem. Soc.* **1978**, *100*, 6093.
(57) Jorgensen, K. A.; Hoffmann, R. *J. Am. Chem. Soc.* **1986**, *108*, 1867.
(58) Dedieu, A.; Albright, T. A.; Hoffmann, R. *J. Am. Chem. Soc.* **1979**, *101*, 3141.
(59) Tatsumi, K.; Hoffmann, R. *J. Am. Chem. Soc.* **1981**, *103*, 3328.
(60) Tatsumi, K.; Hoffmann, R.; Yamamoto, A.; Stille, J. K. *Bull. Chem. Soc. Jpn.* **1981**, *54*, 1857.
(61) Albright, T. A.; Hofman, P.; Hoffmann, R. *J. Am. Chem. Soc.* **1977**, *99*, 7546.

C–M–C (axial) 180°; in Ru compounds with phosphido bridges Ru–P = 2.3 Å; in $Ni_4(\mu\text{-}SH)_8$ Ni–S = 2.2 Å, S–H = 1.4 Å, Ni···Ni = 2.69 Å; in $[Pd_4(\mu\text{-}CO)_4H_8]^{4-}$ Pd–Pd = 2.66 Å, Pd···Pd = 2.91 Å, Pd–C = 2.00 Å.

The three-dimensional graphics of the orbitals has been performed by a computer program named CACAO (Computer Aided Composition of Atomic Orbitals) written in fortran language by C. Mealli and D. M. Proserpio. A detailed description is reported elsewhere.[62]

Acknowledgment. Part of this work was supported by the "Progetto Finalizzato Chimica Fine"—CNR Roma. We are grateful to Prof. Angelo Sironi for helpful discussions and Prof. Roald Hoffmann for encouragement. The e-mail messages of Agustin Ramos at Simon Frazer University are also acknowledged.

(62) Mealli, C.; Proserpio, D. M. *J. Chem. Educ.* **1990**, *66*, 000.